Chinese Chemical Letters 36 (2025) 109965

Contents lists available at ScienceDirect

Chinese Chemical Letters

journal homepage: www.elsevier.com/locate/cclet

Discovery of 3-trifluoromethyl-substituted pyrazoles as selective phosphodiesterase 10A inhibitors for orally attenuating isoprenaline-induced cardiac hypertrophy

Han Yuan[a,1], Fengcai Zhang[a,1], Hongzhe Huang[a,1], Jiafei Wu[a], Yi Yang[a], Wanyi Huang[a], Dongjing Yang[a], Zhuoming Li[a], Zhe Li[a], Ling Huang[b], Yi-You Huang[b,*], Hai-Bin Luo[b,*], Lei Guo[a,*]

[a] School of Pharmaceutical Sciences, Sun Yat-sen University, Guangzhou 510006, China
[b] Key Laboratory of Tropical Biological Resources of Ministry of Education and Hainan Engineering Research Center for Drug Screening and Evaluation, School of Pharmaceutical Sciences, Hainan University, Haikou 570228, China

ARTICLE INFO

Article history:
Received 3 March 2024
Revised 29 April 2024
Accepted 2 May 2024
Available online 3 May 2024

Keywords:
Phosphodiesterase
Inhibitor
Drug design
Isoprenaline
Cardiac hypertrophy

ABSTRACT

Recently, **MP-10**, a previous drug candidate with potent inhibition of phosphodiesterase 10A (PDE10A) in clinical phase II trials for schizophrenia or Alzheimer's disease, has shown significant potential in preventing and treating cardiovascular diseases. However, its poor metabolic stability and high permeability across the blood-brain barrier (BBB) make it unsuitable for preventing and treating peripheral cardiovascular diseases. Herein, the hit-to-lead optimization was performed to discover novel 3-trifluoromethyl-substituted pyrazole derivatives as potent and selective PDE10A inhibitors. The structure-activity relationships, biological characterization, molecular mechanism, and drug-like evaluation were discussed to identify compound **C7** which showed potent inhibition against PDE10A (half maximal inhibitory concentration, $IC_{50} = 11.9$ nmol/L), more than 840-fold selectivity over other PDE subtypes, enhanced liver microsomes stability ($T_{1/2} = 239$ min) compared to **MP-10** and low BBB permeability. Importantly, oral pretreatment with **C7·3HCl** at a dose of 5.0 mg/kg significantly attenuated the pathological and functional changes induced by isoprenaline (ISO)-induced pathological cardiac hypertrophy in mice, particularly suppressing increase of cardiac weight, atrial natriuretic peptide (ANP) and β-myosin heavy chain (β-MHC) hypertrophic markers along with cardiac fibrosis. These findings further support that targeting PDE10A provides an innovative therapeutic approach for preventing and treating cardiac diseases.

The pathological cardiac hypertrophy (CH) is characterized by an aberrant increase in myocardial mass within the left ventricle, and the long-term pathological CH increases demand for myocardial oxygen and subsequent myocardial ischemia, ultimately leading to the development of cardiovascular disease, such as hypertension and heart failure (HF). The progressive exacerbation of cardiac hypertrophy is a significant etiology for the development of heart failure, which impacts estimated 64.3 million individuals globally [1]. The current therapeutic options available for patients with cardiac hypertrophy remain limited, highlighting the urgent need for an effective and targeted therapeutic intervention. The ubiquitous second messengers of cyclic adenosine-3′,5′-monophosphate (cAMP) and cyclic guanosine-3′,5′-monophosphate (cGMP) play a crucial role in intracellular signaling within the field of cardiovascular biology and diseases [2]. The duration, magnitude, and compartmentalization of cyclic nucleotides signaling in the cell are regulated by cyclic nucleotide phosphodiesterases (PDEs) through catalyzing the hydrolysis of cyclic nucleotides. The PDE superfamily in mammals consists of over 100 distinct isoforms, which are categorized into 11 closely related isozymes (PDE1–11) encoded by 21 genes due to alternative splicing and the presence of different translation initiation sites [3]. Among these, PDE1–5 and PDE8–10 have been identified in cardiac tissues [2,4]. The successful utilization of the PDE3 inhibitor (milrinone) in treating acute decompensated HF, along with the effectiveness of PDE5 inhibitors (sildenafil and tadalafil) for pulmonary arterial hypertension, has sparked ongoing interest in novel therapeutic application and development of various PDE inhibitors in combatting cardiovascular diseases (CVDs) [5,6]. Extensive litera-

* Corresponding authors.
E-mail addresses: hyyou@hainanu.edu.cn (Y.-Y. Huang), hbluo@hainanu.edu.cn (H.-B. Luo), guolei7@mail.sysu.edu.cn (L. Guo).
[1] These authors contributed equally to this work.

https://doi.org/10.1016/j.cclet.2024.109965
1001-8417/

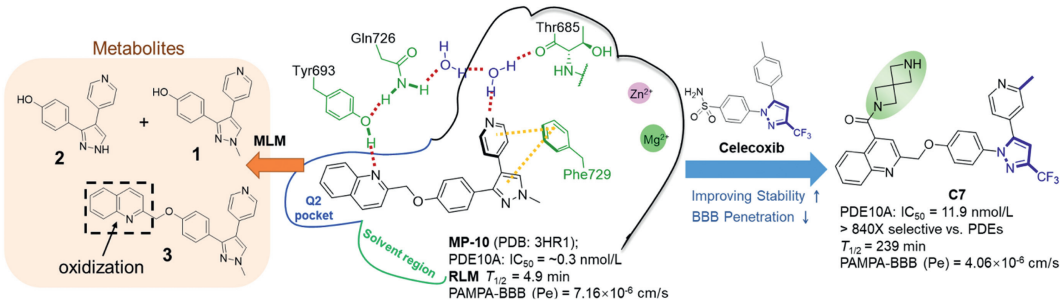

Fig. 1. Structure-based design of 3-trifluoromethyl-substituted pyrazoles as selective PDE10A inhibitors with improved metabolic stability and reduced BBB penetration.

ture supports the notion that dysregulation in the expression, activation, and subcellular localization of PDEs has a significant impact on cardiac function and is associated with pathological conditions such as CH and HF [7]. This underscores the potential of targeting PDEs as therapeutic interventions for cardiac diseases [2,4,6,8].

As a cAMP/cGMP dual-specific PDE, PDE10A exhibits more efficient hydroxylation of cAMP than that of cGMP due to its higher affinity toward cAMP in comparison of cGMP (with a K_m value of 0.26 and 7.2 μmol/L, respectively) [9]. Recently, multiple preclinical studies using animal models have drawn attention to PDE10A as an important regulatory target for the treatment of cardiovascular diseases. PDE10A is significantly upregulated not only in preclinical mouse models of hypertrophy and heart failure, but also in human failing hearts. PDE10A inhibition and deficiency reduce myocardial fibrosis, improve left ventricular function, and attenuate pathological hypertrophy [10]. The crucial role of PDE10A in regulating smooth muscle cell (SMC) proliferation and intimal hyperplasia provides a potential therapeutic strategy for treating vascular occlusive diseases [11]. A central role of PDE10A in progressive pulmonary vascular remodeling highlights the potential of PDE10A inhibitors as an effective therapeutic approach for treating pulmonary arterial hypertension (PAH) [12,13]. Moreover, PDE10A has shown great potential as a therapeutic target due to its well-established safety profile in treating various psychiatric and neurological disorders such as schizophrenia, Alzheimer's disease (AD), Huntington's disease (HD), and Parkinson's disease [14,15]. Therefore, we believe that PDE10A inhibitors have great therapeutic potential for cardiac diseases associated with pathological cardiac remodeling or various CVDs.

Due to the potent inhibitory activity of **TP-10** and **MP-10** against PDE10A, these compounds not only reversed pre-established cardiac hypertrophy and dysfunction but also suppressed smooth muscle cell proliferation and intimal hyperplasia for treating vascular occlusive diseases [10,11]. However, their metabolic stability in mouse liver microsomes (MLM) was extremely poor, as indicated by high intrinsic clearance rate [16]. Moreover, the high permeability across the blood-brain barrier (BBB) exhibited by **TP-10** or **MP-10** made them unsuitable for preventing and treating CVDs, due to the potential risk of causing PDE10A inhibition in the central nervous system (CNS). Herein, we demonstrated that the structure-based design and druglike optimization were utilized to discover 3-trifluoromethyl-substituted pyrazole derivatives as potent and selective PDE10A inhibitors. The structure-activity relationships (SARs) were discussed prior to conducting biological characterization and drug-like evaluation on the lead compound **C7**, which showed potent inhibition against PDE10A with a half maximal inhibitory concentration (IC_{50}) value of 11.9 nmol/L, excellent selectivity (>840-fold) towards other PDE subtypes, and significantly improved rat liver microsomes stability compared to **MP-10**. Furthermore, **C7·3HCl** demonstrated acceptable pharmacokinetic properties enabling its administration *via* oral intake for *in vivo* studies. Importantly, the pretreatment with **C7·3HCl** significantly mitigated the pathological and functional changes caused by isoprenaline (ISO)-induced pathological cardiac hypertrophy in mice at a dosage higher than 5.0 mg/kg (*p.o.*). These findings further support that targeting PDE10A provides an innovative therapeutic approach for preventing and treating cardiac diseases.

Before any attempt at the structure modifications of **MP-10**, molecular docking, and molecular dynamics (MD) simulations were implemented in advance to accelerate the design and optimization process of PDE10A inhibitors with novel scaffolds by virtue of the X-ray cocrystal structure of **MP-10** complex (PDB: 3HR1) [17]. According to this crystallographic study, the quinoline moiety as an effective selective pocket binding group (SPBG) was inserted into the unique selectivity pocket Q2 along with a strong H-bond interaction with Tyr693 in the catalytic domain of the recombinant PDE10A. Therefore, we decided to keep quinoline structure and modify other parts of **MP-10** including pyrazol, phenoxy and pyridyl units, to improve compound stability in rat liver microsomes (RLM). In previous study, there were three major metabolites in mouse liver microsomes including fragment **1** cutting off from **MP-10**, fragment **2** from subsequently demethylation at the pyrazole ring of fragment **1**, and compound **3** probably derived from the quinoline ring oxidation (Fig. 1) [18]. Given the previous guide, a 3-trifluoromethyl-substituted pyrazole scaffold was chosen to replace the 1-methyl-substituted pyrazole moiety of **MP-10**. Because this scaffold inspired from the structure of celecoxib, a well-known non-steroidal anti-inflammatory drug (NSAID), was considered as an excellent bioisosteric group to enhance molecule stability. Because of easy oxidization of the quinoline ring, the strategy of different substituents introduced into 4-position of the quinoline ring was aimed to not only tune compound stability in RLM without affecting the inhibitory activity, but to improve drug-like properties, such as solubility, human ether-à-go-go-related gene (*h*ERG) K^+ channel inhibition and BBB permeability. The purpose of the structural modification on the phenoxy and pyridine units was to reveal potential metabolite sites to improve compound's stability in RLM.

A novel series of 3-trifluoromethyl-substituted pyrazole derivatives coupled with 4-substituted quinoline (A, B and C series) was designed. The binding free energies ($\Delta G_{bind,pred}$) were predicted using a MD simulations approach (MM-PBSA), aiming to accelerate the optimization process. Compared with **MP-10** (-34.90 ± 2.46 kcal/mol), all most of designed compounds showed more negative $\Delta G_{bind,\ pred}$ values, except for compound **B2** (Table S1 in Supporting information). The synthesis of the pyrazole scaffold was performed in two steps (Scheme S1 in Supporting information). At first, the required various trifluoromethyl-1,3-diketones were furnished through a Claisen condensation between ethyl trifluoroacetate and aryl methyl ketones. In the second step, condensations of various trifluoromethyl-1,3-diketones with 4-methoxyphenylhydrazine hydrochloride (or 4-benzyloxyphenylhydrazine hydrochloride) provided different aryl

Table 1
PDE10A inhibitor activity and liver microsomes stability in RLM.

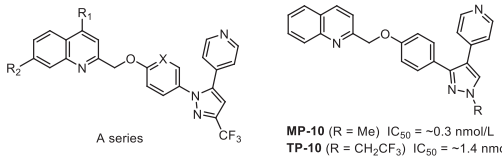

No.	R_1	X	IC_{50} (nmol/L) [a]	$T_{1/2}$ (min) [b]
A1	H	CH	6.3 ± 0.1	18.1
A2		CH	28.7 ± 0.7	—[d]
A3		CH	7.6 ± 0.2	19.7
A4		CH	27.8 ± 2.3	—[d]
A5	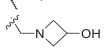	CH	18.0 ± 2.6	—[d]
A6		CH	68.6 ± 11.7	—[d]
A7		CH	5.2 ± 1.1	—[d]
A8		CH	16.6 ± 2.2	8.8
A9	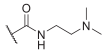	CH	7.2 ± 0.1	20
A10	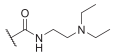	CH	23.1 ± 3.0	27.5
A11	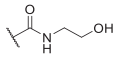	CH	7.7 ± 0.2	25.7
A12	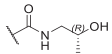	CH	14.1 ± 0.1	—[d]
A13		CH	22.4 ± 0.5	—[d]
A14[c]		CH	19.2 ± 1.8	17.4
A15		CF	22.4 ± 0.5	—[d]
A16		N	> 100 nmol/L	—[d]
MP-10			0.3 ± 0.1[e]	4.9

[a] Data are given as mean ± SD ($n \geq 2$). Papaverine used as a control in tests.
[b] Rat liver microsomes test using phenacetin as reference. The R_2 group of compounds represented the H atom except **A14**.
[c] The R_2 group of **A14** represented the F atom.
[d] Not determined.
[e] **MP-10** as another positive control in tests with an IC_{50} value of 0.3 ± 0.1 nmol/L.

Table 2
PDE10A inhibitor activity and liver microsomes stability in RLM.

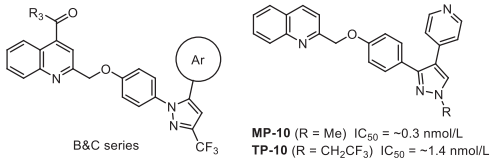

No.	R_3	Ar	IC_{50} (nmol/L) [a]	$T_{1/2}$ (min) [b]
B1	-NHMe		10.2 ± 0.1	—[d]
B2	-NHMe		> 100	—[d]
B3	-NHMe		33.2 ± 0.7	—[d]
B4	-NHMe		> 100	—[d]
B5	-NHMe		58.5 ± 1.6	11
B6	-NHMe		17.2 ± 0.1	—[d]
B7	-NHMe		> 100	83.5
B8	-NHMe		34.4 ± 5.1	38.5
B9	-NHMe		4.0 ± 0 9	99
C1			6.9 ± 0.1	39
C2			11.6 ± 2.0	187
C3	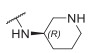		13.3 ± 1.6	24
C4			12.6 ± 2.4	107
C5	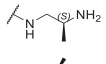		13.0 ± 0.1	43
C6			5.5 ± 0.1	24.8
C7			11.9 ± 1.5	239
MP-10			0.3 ± 0.1[c]	4.9

[a] Data are given as mean ± SD ($n \geq 2$). Papaverine used as a control in tests.
[b] Rat liver microsomes test using phenacetin as reference.
[c] **MP-10** as another positive control in tests with an IC_{50} value of 0.3 ± 0.1 nmol/L.
[d] Not determined.

and heteroaryl substituted trifluoromethyl phenoxy pyrazoles. After deprotection of the methyl or benzyl group, nucleophilic substitution reactions were carried out between different 2-(bromomethyl)quinoline derivatives and phenols in conjunction with 3-trifluoromethyl pyrazole. This resulted in the formation of corresponding 3-trifluoromethyl-substituted pyrazole derivatives combined with 4-substituted quinoline, some of which were evaluated for their potency in inhibiting PDE10A. Other final products were obtained in a similar scheme, additionally followed by hydrolysis, condensation, deprotection, reduction or substitution as illustrated in Schemes S1–S3 (Supporting information).

Our initial efforts focused on modifying position 4 of the quinoline to enhance stability in RLM, based on metabolite analysis of **MP-10** [18]. Various substituents were introduced at position 4 of the quinoline, including dimethylaminomethyl, ketone, carbonyl, carboxamide, and thioamide (Table 1). The results from A series compounds revealed that electron-withdrawing groups at position 4 of the quinoline not only increased inhibitory potency (IC_{50} < 29 nmol/L) but also contributed to the RLM stability of compounds by decreasing electron density of the quinoline ring. As illustrated in Table 1, the side chains of amides introduced at position 4 of the quinoline enhanced the compound stability while maintaining PDE10A inhibitory activity. Among these compounds, **A11** exhibited an enhancement in metabolic stability with a half-life ($T_{1/2}$) of 27.5 min in RLM, better than **MP-10** ($T_{1/2} = 4.9$ min); however, it experienced a decrease in inhibitory potency. The above findings indicate that modifying the quinoline moiety at position 4 can fine-tune the compound's physicochemical properties without significantly compromising its inhibitory potency [13]. Unexpectedly, the introduction of a fluorine atom at the R_2 position resulted in a decrease in inhibitory activity for compound **A14**, with an IC_{50} value of 19.2 nmol/L compared to compound **A3**. Furthermore, replacing the middle phenoxy linker with a (pyridin-2-yl)oxy moiety (**A16**) led to more than a 12-fold decrease in inhibitory potency.

On the other hand, the pyridine moiety connecting to the pyrazole scaffold, which was potentially susceptible to metabolism, was replaced by 4-substituted aromatic or various heteroaryl rings. It is noticeable that this 4-pyridine unit is more favored to maintain activity against PDE10A in contrast with 4-substituted benzenes (**B1** and **B2**), pyridazine, 1-methyl-pyridin-2-one or pyridine *N*-oxide moiety (**B5**–**B7**) in Table 2. In the meanwhile, the pyridyl nitrogen atom is optimally positioned in the *para* position with respect to the 3-trifluoromethyl-substituted pyrazole scaffold, indicating the rank order of PDE10A inhibitory activity as follows: 4-

Table 3
Selectivity profile of **C7** across PDE families.

PDE	IC_{50} (nmol/L)	Selectivity fold[a]
PDE10A2 (449–770)	11.9 ± 1.5	/
PDE1C (151–528)	> 10,000	> 840
PDE2A (580–919)	> 10,000	> 840
PDE3A (679–1087)	> 10,000	> 840
PDE4D2 (286–413)	> 10,000	> 840
PDE5A1 (535–860)	> 10,000	> 840
PDE6C (1 – 858)	> 10,000	> 840
PDE7A1 (130–482)	> 10,000	> 840
PDE8A1 (480–820)	> 10,000	> 840
PDE9A2 (181–506)	> 10,000	> 840
PDE11A4 (588–911)	> 10,000	> 840

[a] Selectivity fold = IC_{50}(PDEs)/IC_{50}(PDE10A2).

pyridyl > 3-pyridyl > 2-pyridyl. It is worth noting that the pyridine *N*-oxide derivative (**B7**) demonstrated a significant enhancement in microsomes stability (RLM $T_{1/2}$ = 83.5 min) compared to **A3** (RLM $T_{1/2}$ = 19.7 min), despite experiencing a notable loss of inhibitory activity. This finding indicates that the metabolic instability is attributed to the oxidation of unencumbered nitrogen of the pyridine binding to the heme of CYP450 [16]. However, preserving inhibitory activity while enhancing metabolic stability is challenging due to the crucial role of the N atom fixed at position 4 of the pyridine ring. Fortunately, modifying the pyridine ring with a methyl group adjacent to the N atom (**B9**) significantly enhanced compound stability without loss of inhibitory activity against PDE10A. The reason is probably that the methyl group's steric hindrance impedes the liver microsomal enzyme's oxidation catalytic center from oxidizing the N atom of the pyridine ring.

Given the favorable tolerability of introducing a carboxamide at position 4 of the quinoline moiety in terms of PDE10A inhibitory activity and stability enhancement, a series of compounds incorporating various amines in series C were obtained. Apparently, the potency trend of pyrrolidine > piperidine ≈ ethanediamine/2-hydroxyethylamine was observed in the case of **C1**, **C2**, **C3** and **C5**, indicating the cyclic amine moieties exhibited better inhibition potency. Interestingly, the side chains of cyclic amines exhibited superior liver microsomes stability among **C1–C5** and **C7**. Surprisingly, compound **C6**, containing 4,7-diazaspiro[2.5]octane, showed excellent inhibitory potency against PDE10A but lacked remarkable metabolic stability compared to **C4**. On the other hand, compound **C7** containing rigid 2,6-diazaspiro[3.3]heptane demonstrated remarkable rat liver microsomes stability ($T_{1/2}$ = 239 min).

The initial study successfully identified potent PDE10A inhibitors, such as **C1–C3**, **C6** and **C7**, with favorable liver microsomes stability. However, it is crucial to select the most suitable candidate among them for further evaluation of physicochemical properties. Suppression of the *h*ERG K^+ channel is associated with cardiotoxicity [19] and taken into consideration for drug safety evaluation as shown in Table S3 (Supporting information). The results suggested that the choice of flexible amide side chains in this series of compounds significantly impacted the inhibition of *h*ERG K^+ channels (**A3** *vs.* **A9**). To improve *h*ERG profiles, C series compounds containing cyclic amides or amides with cyclic amines were designed and roughly evaluated for *h*ERG inhibition using an automated Qpatch-clamp electrophysiology assay. Notably, amide side chains coupled with pyrrolidine, piperidine, or piperazine moiety were not adequate to attenuate *h*ERG inhibition compared to **A3** in Table S3 (Supporting information), while compound **C7** with rigid 2,6-diazaspiro[3.3]heptane exhibited faint inhibition of the *h*ERG K^+ channel (IC_{50} = 10.9 μmol/L) *in vitro*. Thus, compound **C7** was subsequently subjected to further evaluations.

The selectivity profile of compound **C7** against other PDE isoforms is summarized in Table 3. Compound **C7** with an IC_{50} value of 11.9 nmol/L against PDE10A2 exhibited weak inhibition (lower than 50% inhibition rate at 10 μmol/L) towards most of the representative PDE subtypes including PDE1–9 and PDE11, indicating its excellent selectivity index across the PDE family. This high selectivity across the PDE family can be attributed to the quinoline fragment of **C7** effectively occupying the narrow Q2 pocket of PDE10A and maintaining a strong H-bond interaction with Try693. Therefore, compound **C7** is suitable for further development as a lead compound.

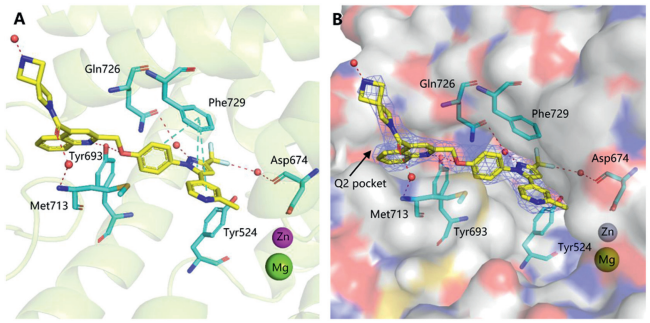

Fig. 2. Crystal structure of PDE10A catalytic domain in complex with compound **C7** (PDB ID: 8XV3). (A) Ribbon model of **C7** binding in the active site of PDE10A. (B) Surface presentation, the $2F_o$-F_c electron density is contoured in blue at 1.0 σ. The protein and **C7** are shown as a stick model with cyan and yellow C atoms, respectively. The red and green dash lines indicate H-bond interactions and multiple π-π interactions, respectively. Red balls represent water molecules.

The X-ray crystal structure of PDE10A2 catalytic domain (residues 449–779) in complex with **C7** was determined at 2.3 Å resolution and deposited in the Protein Data Bank (PDB: 8XV3). Residues are numbered as in the PDE10A2 splice variant (UniprotQ9Y233–2). The profile of the PDE10A-**C7** complex exhibited a distinct outward extension of α-methylpyridine, which clearly differed from that of **MP-10** (PDB: 3HR1) [17], where the same pyridine moiety extended inside into the pocket as illustrated in Fig. 1. The trifluoromethyl group on the pyrazol unit of **C7** preferred to internal extension, thereby engaging in water-mediated halogen bonding interactions with Asp674 within the H-pocket. In addition, the pyrazole unit of **C7** exhibited a water-mediated hydrogen bond interaction with the conserved Gln726. The quinoline moiety was inserted into the "selective Q2 pocket" and established a hydrogen bond interaction with Tyr693, which concomitantly formed an additional hydrogen bond with the oxygen atom of the phenoxy group (Fig. 2A) [20]. The residue Phe729 played a crucial role by engaging in $\pi-\pi$ interaction with both pyrazole and α-methylpyridine of **C7**, while simultaneously forming edge-to-side $\pi-\pi$ stacking with the middle linkage benzene ring of **C7** (green dash line). This new binding pattern as illustrated by crystal structure explained that certain compounds lacking significant PDE10A inhibitory activity probably did not align with the predicted modes utilized by our MD simulations approach.

In consideration of its potent inhibition against PDE10A and remarkable selectivity across various PDE isoforms, **C7** underwent comprehensive druglike analysis including *t*PSA and clog*P* calculation, water solubility, human plasma protein binding rate, cytochrome P450 inhibition potential, assessments of blood-brain barrier (BBB) permeability and oral bioavailability. The drug-like properties of **C7** were presented in Table S5 (Supporting information). These encompass its aqueous solubility, metabolic stability ($T_{1/2}$ = 239 min) in RLM, human plasma protein binding affinity (PPB = 98.4%), inhibition potential against cytochrome P450 enzymes (CYP1A2, 2C9, 2C19, 2D6, and 3A4-M), *h*ERG inhibition (IC_{50} = 10.9 μmol/L) as well as acute oral toxicity. The oral administration of **C7·3HCl** to mouse resulted in an approximate half-life ($t_{1/2}$, *in vivo*) of 6.2 h and an oral bioavailability of ~18.8%. More-

over, the predicted topological polar surface area (*t*PSA) and clog*P* values for **C7** fall within the appropriate range for druggability. The BBB permeability of **C7**, as determined by the standard curve in the parallel artificial membrane permeation assay (PAMPA), was calculated to be as low as 4.06×10^{-6} cm/s, implying that it was not suitable as a CNS compound (Table S7 in Supporting information) [21]. This suggested that **C7** exhibited suitability to be investigated for peripheral cardiac diseases.

In this study, all animal care and experimental protocols were in accordance with the "Guide for the Care and Use of Laboratory Animals" (National Institutes of Health Publication, revised 1996, No. 86–23, Bethesda, MD) and approved by the Institutional Ethical Committee for Animal Research of Sun Yat-sen University (IACUC number: SYSU-IACUC-2023001861). Different dosage regimens (2.5, 5.0, and 10 mg kg^{-1} d^{-1} for two weeks) of compound **C7·3HCl** were orally administrated to an ISO-induced cardiac hypertrophic C57BL/6J mouse model (at age 8–10 weeks) in the comparison with propranolol (10 mg kg^{-1} d^{-1}, *p.o.*). ISO is a β-adrenoceptor agonist widely used to rapidly induce CH. The subcutaneous administration of ISO at a dosage of 5.0 mg kg^{-1} d^{-1} throughout the study led to significant cardiac hypertrophy when compared to the control group, as indicated by an increased ratio of heart weight/body weight (HW/BW) and heart weight/tibia length (HW/TL) (Figs. 3A and B), elevated expression levels of atrial natriuretic peptide (ANP) and β-myosin heavy chain (β-MHC) as markers for cardiac hypertrophy genes (Figs. 3C and D), along with an enlarged cross-sectional area of cardiomyocytes observed through wheat germ agglutinin (WGA) staining analysis (Fig. 3F). Compound **C7** effectively decreased these ratios nearly in a dose-dependent manner when compared with ISO animals. Both HW/BW and HW/TL ratios improved upon **C7** treatment. The levels of ANP and β-MHC were significantly increased in the ISO group, as revealed by quantitative real-time polymerase chain reaction (qRT-PCR), while their expression was significantly inhibited by **C7**, seemingly surpassing those results of the propranolol group in the same dosage. In the ISO group, there was a significant increase in cardiomyocyte areas during 14 days, whereas treatments with **C7** effectively suppressed this elevation comparable to that of the propranolol in the same dosage (Fig. 3F). Moreover, picrosirius red staining revealed a significant deposition of cardiac collagen in ISO-induced hypertrophied hearts. However, treatment with **C7** noticeably reduced the fibrotic area of the heart as indicated by picrosirius red-positive area staining (Fig. 3G), suggesting a remarkable anti-myocardial fibrosis effect. Additionally, compound **C7** significantly increased the expression levels of cAMP in the heart tissues, while propranolol did not adequately exhibit this enhancement (Fig. S1 in Supporting information). This implied that the cardioprotective effects of compound **C7** was likely attributed to its regulation of a cAMP/PKA signaling pathway.

Cardiac function was assessed through echocardiographic analysis, encompassing the evaluation of left ventricular ejection fraction (EF), fractional shortening (FS), end-diastolic (LVIDd) and end-systolic (LVIDs) left ventricular inner diameters, as well as end-diastolic (LVEDv) and end-systolic (LVESv) left ventricular volumes following the final administration. As expected, ISO-induced cardiac hypertrophy in mice led to cardiac dysfunction characterized by reduced EF and FS, as well as increased LVIDs, LVIDd, LVEDv, and LVESv (Fig. 4). Nevertheless, the echocardiography showed significant improvements in cardiac function upon **C7** treatment. In particular, the oral administration of **C7** in a dose-dependent manner effectively enhanced the reduction of EF, as compared to the ISO group. The left ventricular remodeling was ameliorated, as evidenced by reductions in both left ventricular inner diameters and volumes. Since the role of PDE10A induction in promoting cardiac hypertrophy, fibrosis, and dysfunction has been demonstrated [10], compound **C7** has potentials to attenuate cardiac hypertrophy and

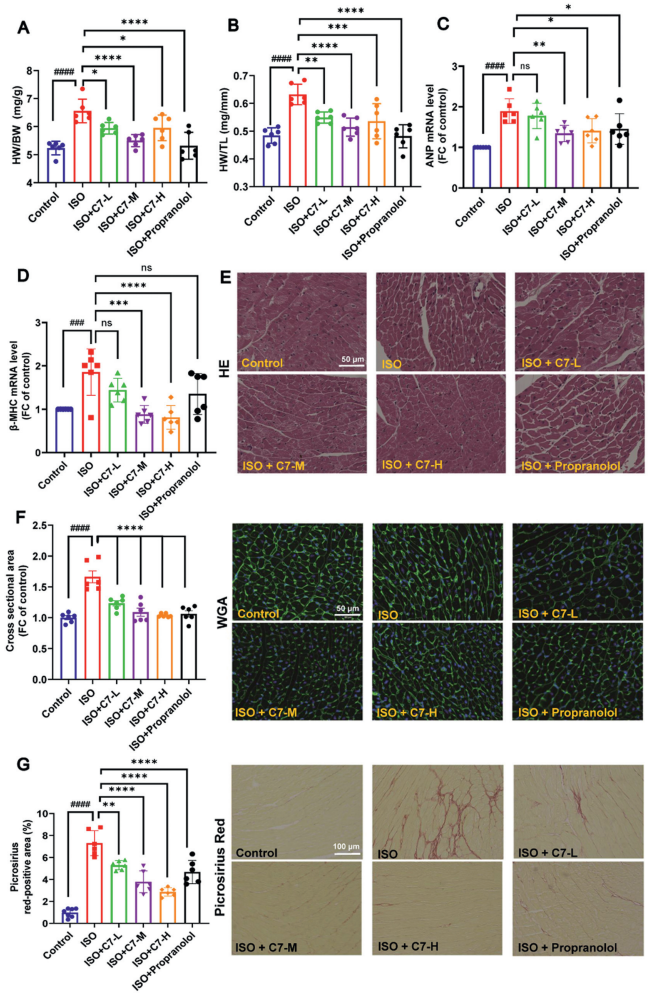

Fig. 3. Compound **C7** effectively reduced isoprenaline-induced CH at various oral dosages (L, M, H: 2.5, 5.0 and 10 mg kg^{-1} d^{-1}, respectively) comparing with propranolol (10 mg kg^{-1} d^{-1}, *p.o.*) during 14 days while maintaining continuous co-treatment with subcutaneous injections of ISO at a dosage of 5.0 mg kg^{-1} d^{-1} throughout. (A) HW/BW. (B) HW/TL. The mRNA expressions of hypertrophy markers, including ANP (C) and β-MHC (D), respectively, quantified through qRT-PCR ($n = 6$). (E) Representative hematoxylin staining images of control, ISO, **C7** and propranolol heart tissue at 14 days. Scale bar: 50 μm. (F) WGA staining images of control, ISO, **C7** and propranolol heart tissue at 14 days; Quantitative data of CM hypertrophy assessed by cross-sectional area of WGA staining ($n = 6$ hearts per group with ~100 CMs analyzed per heart. Scale bar: 50 μm. (G) Representative picrosirius red staining images and analysis of cardiac fibrosis area in cardiac tissues ($n = 6$). Quantification of total fibrosis of representative images of heart sections stained with picrosirius red ($n = 6$). Red staining shows fibrotic areas. Scale bar: 100 μm. Data were presented as the mean ± SEM. $^{###}P < 0.001$, $^{####}P < 0.0001$ *vs.* the control group; $^{*}P < 0.05$, $^{**}P < 0.01$, $^{***}P < 0.001$, $^{****}P < 0.0001$ *vs.* the ISO group. ns means no significance.

improve pathological ventricular remodeling with anti-myocardial fibrosis effect *in vivo* in light of our findings, which highlight that inhibiting PDE10A may be a promising therapeutic approach for preventing and treating cardiac diseases associated with adverse cardiac hypertrophy.

In summary, recent groundbreaking research has shown the remarkable potential of highly potent PDE10A inhibitors in preventing and treating cardiac disease and CVDs, in addition to clinic trials for various psychiatric and neurological conditions, such as **TP-10** or **MP-10**. However, their poor metabolic stability and high BBB permeability make them unsuitable for treating CVDs. Herein, the structure-based design/optimization strategy was employed to discover 3-trifluoromethyl-substituted pyrazole derivatives as po-

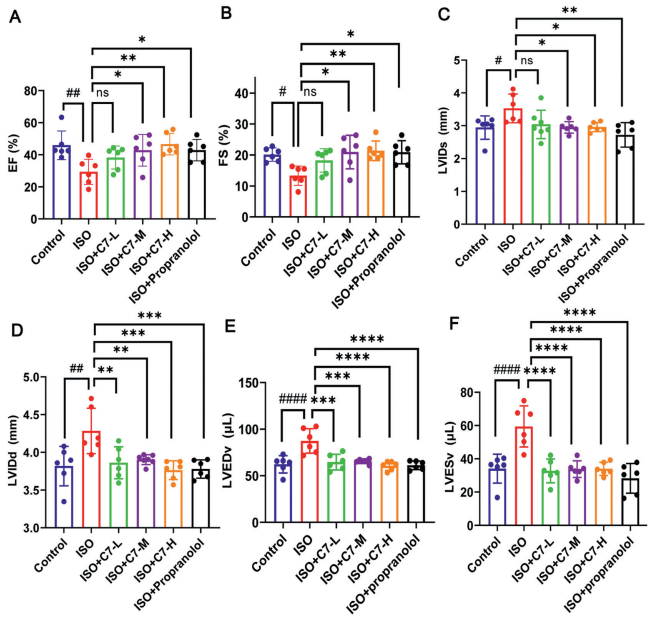

Fig. 4. The effects of **C7** on cardiac function by echocardiography. (A, B) The echocardiographic parameters of left ventricular EF and FS in mice on day 14 ($n = 6$). (C, D) The echocardiographic parameters of LVIDd and LVIDs ($n = 6$) on day 14. (E, F) The echocardiographic parameters of LVEDv and LVESv ($n = 6$) on day 14. Data were presented as the mean ± SEM. $^{\#}P < 0.05$, $^{\#\#}P < 0.01$, $^{\#\#\#}P < 0.001$, $^{\#\#\#\#}P < 0.0001$ *vs.* the control group; $^{*}P < 0.05$, $^{**}P < 0.01$, $^{***}P < 0.001$, $^{****}P < 0.0001$ *vs.* the ISO group.

tent and selective PDE10A inhibitors. The SARs, biological characterization, molecular mechanism and drug-like evaluation were discussed to identify the lead compound **C7** with an IC_{50} value of 11.9 nmol/L, over 840-fold PDEs selectivity, significant enhancement of liver microsomes stability and reduced BBB permeability. The crystal structure of the PDE10A-**C7** complex illustrated a new binding model different from that of **MP-10**, which provided a guideline for rational design of highly selective PDE10A inhibitors. Importantly, oral administration of **C7·3HCl** at a dose of 5.0 mg/kg once daily significantly attenuated the pathological and functional changes induced by ISO-induced pathological cardiac hypertrophy in mice, particularly suppressing increase of cardiac weight, ANP and β-MHC hypertrophic markers induction, as well as cardiac fibrosis. These findings further highlight that inhibiting PDE10A may be a promising therapeutic approach for preventing and treating cardiac diseases associated with cardiac hypertrophy.

Declaration of competing interest

The authors declare that they have no known competing financial interests or personal relationships that could have appeared to influence the work reported in this paper.

CRediT authorship contribution statement

Han Yuan: Methodology, Formal analysis, Data curation. **Fengcai Zhang:** Methodology, Formal analysis, Data curation. **Hongzhe Huang:** Methodology, Formal analysis, Data curation. **Jiafei Wu:** Data curation. **Yi Yang:** Data curation. **Wanyi Huang:** Data curation. **Dongjing Yang:** Formal analysis, Data curation. **Zhuoming Li:** Resources, Conceptualization. **Zhe Li:** Software, Resources, Funding acquisition. **Ling Huang:** Conceptualization. **Yi-You Huang:** Resources, Methodology, Funding acquisition. **Hai-Bin Luo:** Writing – review & editing, Validation, Conceptualization. **Lei Guo:** Writing – review & editing, Writing – original draft, Validation, Supervision, Resources, Project administration, Methodology, Funding acquisition, Conceptualization.

Acknowledgments

This work was supported by the National Natural Science Foundation of China (Nos. 22277154, 82003576, 82273856, 22277019, 22077143, 22377023, 82273925), Natural Science Foundation of Guangdong Province (No. 2021A1515012499), Fundamental Research Funds for Hainan University (Nos. KYQD(ZR)−21031, KYQD(ZR)−21108, KYQD(ZR)−23003, XTCX2022JKA01), Natural Science Foundation of Hainan Province (Nos. KJRC2023B10, 822MS051, 824YXQN420, 324MS018).

Supplementary materials

Supplementary material associated with this article can be found, in the online version, at doi:10.1016/j.cclet.2024.109965.

References

[1] A. Groenewegen, F.H. Rutten, A. Mosterd, A.W. Hoes, Eur. J. Heart Fail. 22 (2020) 1342–1356.
[2] R. Kamel, J. Leroy, G. Vandecasteele, R. Fischmeister, Nat. Rev. Cardiol. 20 (2023) 90–108.
[3] C. Jansen, A.J. Kooistra, G.K. Kanev, et al., J. Med. Chem. 59 (2016) 7029–7065.
[4] S. Chen, C. Yan, Expert Opin. Drug Discov. 16 (2021) 183–196.
[5] N.F. Nadur, L.L. de Azevedo, L. Caruso, et al., Eur. J. Med. Chem. 212 (2021) 113123.
[6] M.E.J. Preedy, Cardiovasc. Drugs Ther. 34 (2020) 401–417.
[7] Q. Fu, Y. Wang, C. Yan, Y.K. Xiang, Physiol. Rev. 104 (2023) 765–834.
[8] P. Bobin, M. Belacel-Ouari, I. Bedioune, et al., Arch. Cardiovasc. Dis. 109 (2016) 431–443.
[9] K. Fujishige, J. Kotera, H. Michibata, et al., J. Biol. Chem. 274 (1999) 18438–18445.
[10] S. Chen, Y. Zhang, J.K. Lighthouse, et al., Circulation 141 (2020) 217–233.
[11] L. Luo, Y. Cai, Y. Zhang, et al., Cardiovasc. Res. 118 (2022) 2703–2717.
[12] X. Tian, C. Vroom, H.A. Ghofrani, et al., PLoS One 6 (2011) e18136.
[13] Y. Yang, S. Zhang, Q. Zhou, et al., Acta Pharm. Sin. B 10 (2020) 2339–2347.
[14] H.S. Amin, P.K. Parikh, M.D. Ghate, Eur. J. Med. Chem. 214 (2021) 113155.
[15] H. Geerts, A. Spiros, P. Roberts, Expert Rev. Neurother. 17 (2017) 553–560.
[16] W. Hamaguchi, N. Masuda, S. Miyamoto, et al., Bioorg. Med. Chem. 23 (2015) 297–313.
[17] P.R. Verhoest, D.S. Chapin, M. Corman, et al., J. Med. Chem. 52 (2009) 5188–5196.
[18] W. Hamaguchi, N. Masuda, K. Samizu, et al., Chem. Pharm. Bull. 62 (2014) 1200–1213.
[19] A. Garrido, A. Lepailleur, S.M. Mignani, P. Dallemagne, C. Rochais, Eur. J. Med. Chem. 195 (2020) 112290.
[20] T.A. Chappie, C.J. Helal, X. Hou, J. Med. Chem. 55 (2012) 7299–7331.
[21] L. Di, E.H. Kerns, K. Fan, O.J. McConnell, G.T. Carter, Eur. J. Med. Chem. 38 (2003) 223–232.